Biochemical and Biophysical Research Communications 460 (2015) 543–548

Contents lists available at ScienceDirect

Biochemical and Biophysical Research Communications

journal homepage: www.elsevier.com/locate/ybbrc

Activation of latent metastases in the lung after resection of a metastatic lymph node in a lymph node metastasis mouse model

Lenan Shao [a, b], Tomoki Ouchi [a], Maya Sakamoto [c], Shiro Mori [a, d], Tetsuya Kodama [a, *]

[a] Laboratory of Biomedical Engineering for Cancer, Department of Biomedical Engineering, Graduate School of Biomedical Engineering, Tohoku University, 4-1 Seiryo, Aoba, Sendai, Miyagi 980-8575, Japan
[b] Department of Oral and Maxillofacial Surgery, Tongji Hospital, Huazhong University of Science and Technology, 1095 Jiefang Avenue, Wuhan 430030, China
[c] Department of Oral Diagnosis, Tohoku University Hospital, 1-1 Seiryo, Aoba, Sendai 980-8575, Japan
[d] Department of Oral and Maxillofacial Surgery, Tohoku University Hospital, 1-1 Seiryo, Aoba, Sendai 980-8575, Japan

ARTICLE INFO

Article history:
Received 8 March 2015
Available online 27 March 2015

Keywords:
Lymph node resection
Distant metastasis
Metastatic mouse model
Latent tumor cells

ABSTRACT

Iatrogenic induction of regional and distant cancer metastases is a risk associated with clinical resection of tumor-positive sentinel lymph nodes. However, there have been no studies of this risk in a mouse model of cancer metastasis. Here, we report that resection of a tumor-bearing subiliac lymph node (SiLN) enhanced lung metastasis in a mouse model of lymph node metastasis. Bioluminescence imaging revealed that metastatic tumor cells in the secondary lymph node continued to grow after resection of the SiLN, and that the probability of metastasis to the lungs was increased when the interval between SiLN inoculation and resection was reduced. Futhermore, histological analysis demonstrated that latents in the lung were stimulated to grow after resection of the SiLN. Fluorescence imaging indicated that the route of tumor cell dissemination from SiLN to the lung was the venous system located over the SiLN. We speculate that our mouse model will be useful for studying the mechanisms of tumor cell latency, with a view to improving the detection and treatment of latent metastases.

1. Introduction

Lymph node (LN) metastasis is an important prognostic factor for many malignant tumors, including breast, head and neck cancers, and plays an important role in the development of distant metastases to vital organs [1]. The treatment of LN metastasis with LN resection is limited to those patients who can tolerate surgery and where the risk of metastatic foci invading other major organs is minimal [2]. Although the area of dissection is determined by clinicopathological guidelines, dissection alone does not control local recurrence in progressive cases and thus is used together with adjuvant therapy. Although dissection of the primary tumor is beneficial, it may disturb metastatic homeostasis [3], resulting in the activation and rapid growth of latent tumors in distant metastases; this has been suggested to occur for several cancer types including breast [4], lung [5] and head and neck [6] cancers. Recurrence after dissection is a common phenomenon, but the underlying mechanisms are not fully understood. Removal of LNs that have an immunological anti-tumor immune role [7] may facilitate the rapid growth of distant latent metastases. However, there are no reports on the relationship between resection of LNs and the subsequent rapid growth of latent micrometastases, for reasons including the microscopic size of tumors, clinical accessibility and the lack of an experimental model.

We have developed mouse models of LN metastasis using MXH10/Mo-*lpr*/*lpr* (MXH10/Mo/lpr) [8]. These models have been used to map the lymphatic system [8], demonstrate the plausibility of administering local therapy to a metastatic LN [9], and shown that a lymphatic drug delivery system can be used to deliver agents to LNs outwit the dissection area [2].

In our study, MXH10/Mo/lpr mice were used as an experimental model of metastasis to show that dissection of a SiLN inoculated with tumor cells resulted in the rapid growth of latent lung tumors. For previously discussed reasons we used the nomenclature “SiLN” instead of “inguinal LN” [8,10].

* Corresponding author. Laboratory of Biomedical Engineering for Cancer, Biomedical Engineering Cancer Research Center, Graduate School of Biomedical Engineering, Tohoku University, 4-1 Seiryo, Aoba Ward, Sendai, Miyagi 980-8575, Japan. Fax: +81 22 717 7583.
E-mail address: kodama@bme.tohoku.ac.jp (T. Kodama).

http://dx.doi.org/10.1016/j.bbrc.2015.03.066
0006-291X/

2. Materials and methods

The Institutional Animal Care and Use Committee of Tohoku University approved all *in vivo* studies.

2.1. Mice

MXH10/Mo/lpr mice (16–18 weeks of age) were bred under pathogen-free conditions in the Animal Research Institute, Tohoku University [8]. MXH10/Mo/lpr mice are unique; their most peripheral LNs grow to 10 mm in size at 2.5–3 months of age and the mice do not develop severe autoimmune diseases.

2.2. Cell culture

Malignant fibrous histiocytoma-like KM-Luc/GFP cells, stably expressing a fusion of luciferase and enhanced-green fluorescent protein genes and C3H/He mouse mammary carcinoma cells (FM3A-Luc), stably expressing the Luc gene, were used [8,11]. The relative growth rates of KM-Luc/GFP and FM3A-Luc cells were 3.8/day and 1.1/day, respectively.

2.3. Visualization of flows into the efferent LVs and the thoracoepigastric vein from the SiLN

Two kinds of dyes were used; India ink and 0.5 mM 5(6)-carboxyfluorescein (MW: 376; excitation: 492 nm; emission: 517 nm; Sigma-Aldrich Japan, Tokyo, Japan). The former was used to identify, visually, communication between the lymphatic and venous system via SiLN, while the latter was used to visualize dynamically the flow from the SiLN to the lymphatic and venous system. A 1-mL syringe connected to a 27-gauge standard double-wing needle (Terumo Co., Tokyo, Japan) was filled with the appropriate solution. To gain access to the LNs, a skin incision was performed under general anesthesia. The solution (60 μL) was injected near the center of the SiLN manually (India ink) or at a rate of 100 μL/min using a driven syringe pump (fluorescence solution). Images were obtained immediately after the injections using a stereomicroscope (SZX10, Olympus, Tokyo, Japan) for India ink or a fluorescence stereomicroscope (M165-FC; fluorescent filter: GFP2; excitation: 460–500 nm; emission: >510 nm; Leica, Bensheim, Germany) connected to a high-speed camera (Cool SNAP HQ2; Photometrics, Tokyo, Japan) for fluorescence solution [2].

2.4. Induction of metastasis to the proper axillary LN by injection of tumor cells into the subiliac LN

KM-Luc/GFP and FM3A-Luc cells passaged three times were used. KM-Luc/GFP (1.0×10^6 cells/mL) or FM3A-luc (1.35×10^7 cells/mL) cells were suspended in a mixture of 20 μL phosphate-buffered saline (PBS) and 40 μL of 400 mg/mL Matrigel (Collaborative Biomedical Products). The SiLN was exposed by incision of the overlying skin, and the lymphatic vessels (LVs) connecting the SiLN to the proper axillary LN (PALN) were clamped (DDP-09-151 clamp; Daddy D Pro, Pakistan). Prepared cells were injected into the cortical part of the SiLN using a 27-G injection needle. The needle was maintained in the same position for 5 min to solidify the Matrigel after removal of the needle. Then, the exposed SiLN was irrigated with 20 mL of saline and excess fluid aspirated (M-20 aspirator; Tokyo M.I. Company, Inc., Japan). Thereafter, the clamp was removed. Subsequently, the wound was sutured with 5–0 polyamide sutures.

2.5. Resection of the SiLN

Mice were anesthetized using an inhaled mixture of 2% isoflurane and oxygen. After depilation and skin disinfection, a minimal invasive approach was used for skin incision and exposure

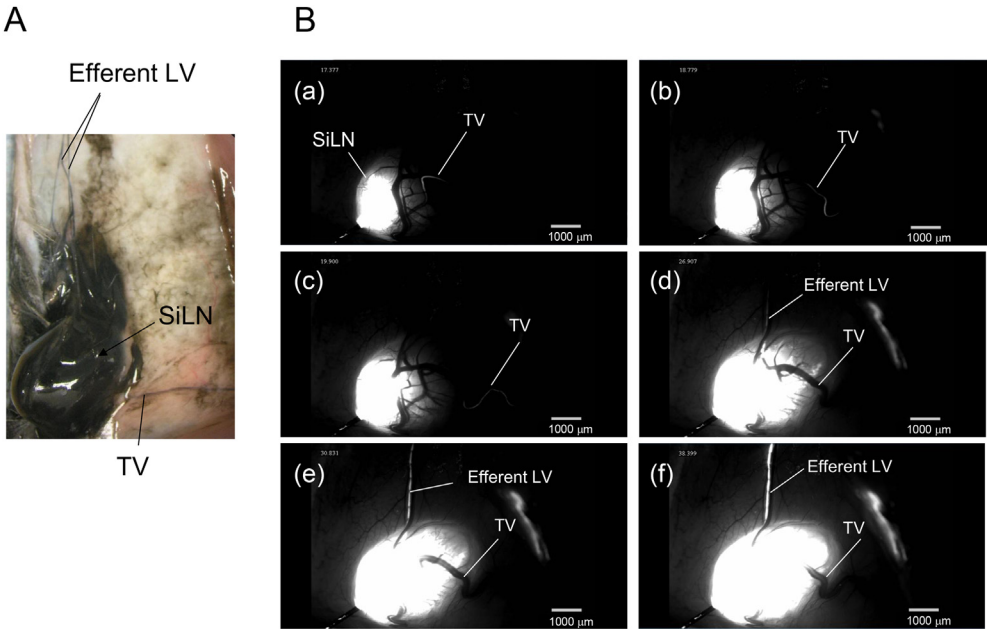

Fig. 1. Communication between the efferent LV and the TV via. SiLN. A. Communication between the efferent LVs and the TV via. SiLN. India ink that was injected into the SiLN flowed into the efferent LVs and the TV. B. Sequential frames from Media 1. Fluorescence solution flowed into the efferent LV and the TV of SiLN. The solution (60 μL) was injected near the center of the SiLN at a velocity of 50 μL/min using a driven syringe pump. (a) 17 s, (b) 19 s, (c) 20 s, (d) 27 s, (e) 31 s, (f) 38 s after the start of recording. Fluorescence solution that was injected into the SiLN flowed into the TV located on the SiLN in (a) and it flowed into the efferent LN in (d). The solution continued to flow from the SiLN into the efferent LVs and TV even in (f).

and extirpation of the SiLN. A bipolar coagulator (Erbotom VI050C; ERBE Elektromedizin GmbH, Germany) and surgical microscope (Leica M80; Leica Microsystems GmbH, Germany) were used to facilitate the SiLN resection process. After excision of the SiLN, the surgical area was washed thoroughly with 20 mL of saline (37 °C) to remove any tumor cells that had leaked from the SiLN. The skin wound was closed with 5–0 polyamide-interrupted sutures. The entire resection procedure was accomplished in 10–15 min.

2.6. Assessment of tumor/metastasis development through measurement of luciferase activity

Tumor development in the SiLN and metastasis to the PALN and lungs were detected using an *in vivo* bioluminescence imaging system (IVIS; Xenogen, USA) [11]. This procedure was carried out separately at 6 h, 3 days, 6 days and 9 days post-inoculation of KM-Luc/GFP cells into the SiLN, and at 6 h, 3 days, 7 days, 14 days, 21 days and 28 days post-inoculation of FM3A-Luc cells into the SiLN. For KM-Luc/GFP cells, the mice were divided into 4 experimental groups: G-C (control; $n = 7$); G-H6 (SiLN dissected 6 h post-inoculation; $n = 8$); G-D3 (SiLN dissected 3 days post-inoculation; $n = 4$); and G-D6 (SiLN dissected 6 days post-inoculation; $n = 5$). The luciferase activities of the dissected LNs and lungs were measured *ex vivo* by IVIS on day 9. For FM3A-Luc cells, mice were divided into 3 groups: G-C (control; $n = 5$); G-H6 (SiLN dissected 6 h post-inoculation; $n = 3$); and G-D21 (SiLN dissected 21 days post-inoculation; $n = 3$). The luciferase activities of dissected LNs and lungs were measured *ex vivo* by IVIS on day 28.

2.7. Histological analysis

Samples of KM-Luc/GFP cells were harvested on day 9 and FM3A-Luc cells on day 28. All samples were fixed in 10% formaldehyde in PBS for 4 days at 4 °C, dehydrated, and then embedded in paraffin. Specimens were cut into 2–4 μm serial sections and stained with hematoxylin and eosin (HE) or elastic-Masson (EM), or immunostained for detection of LYVE-1-positive and CD31-positive cells [11].

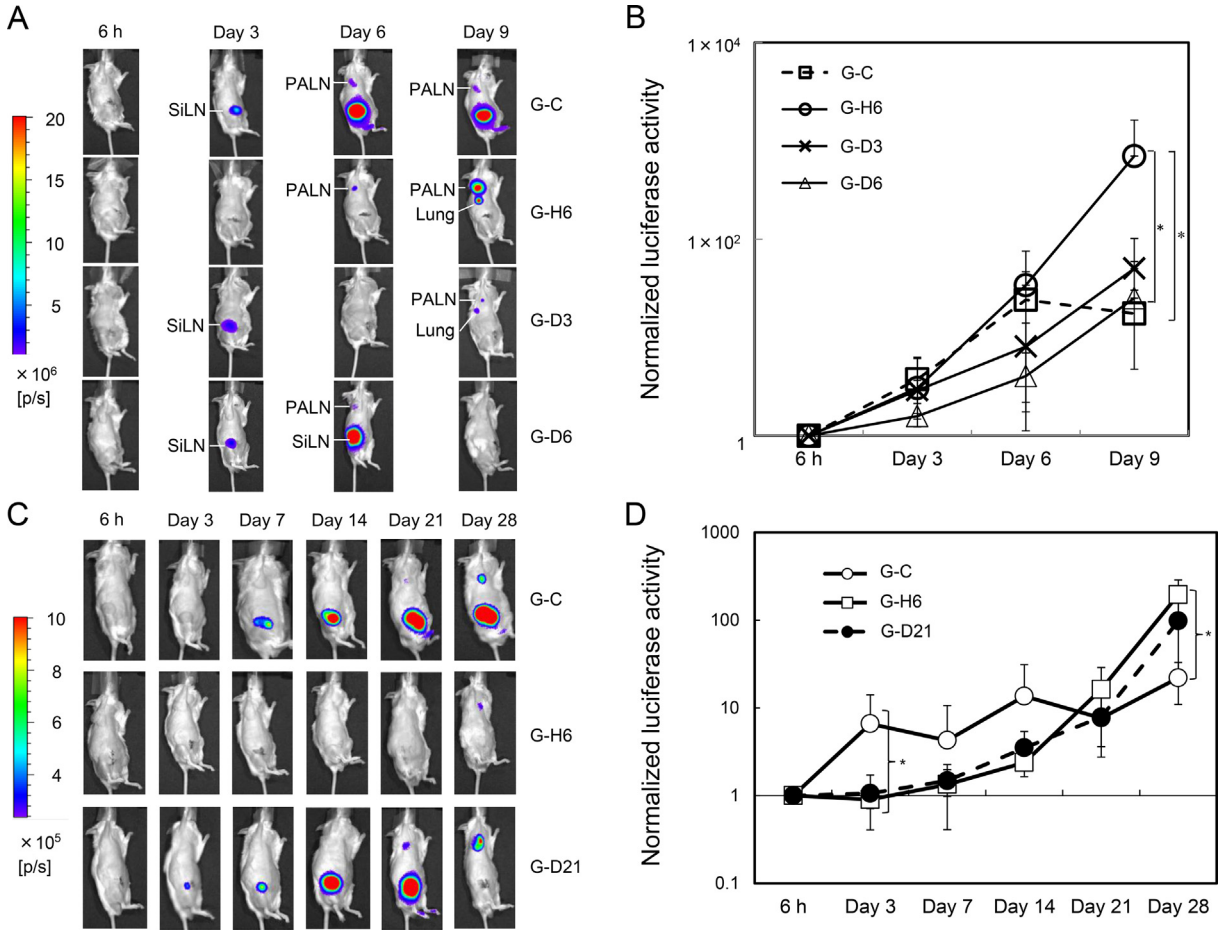

Fig. 2. Luciferase activity in the SiLN and PALN after removal of the SiLN. A, B: KM-Luc/GFP cells were injected into the SiLN ($n = 24$). The SiLN was resected 6 h (G-H6 group, $n = 8$), 3 days (G-D3 group, $n = 4$) or 6 days (G-D6 group, $n = 5$) after tumor cell implantation. SiLNs that were injected with KM-Luc/GFP cells but not removed were used as control samples (G-C group, $n = 7$). (A) Mice after resection of SiLNs. Metastases were detected in the PALN and lungs. Luciferase activity was not detected in the region of the SiLN after the SiLN had been resected. (B) Temporal changes in the luciferase activity of the PALN after resection of the SiLN. The luciferase activity of each group was normalized to that of the mean value at 6 h. G-H6 versus G-C, $P < 0.05$ on day 9; G-H6 versus G-D6, $P < 0.05$ on day 9; Mann–Whitney U-test. C, D: FM3A-Luc cells were injected into the SiLN ($n = 11$). The SiLN was removed 6 h (G-H6 group, $n = 3$) or 21 days (G-D21 group, $n = 3$) after tumor cell implantation. SiLNs injected with cells but not resected were used as control samples (G-C group, $n = 5$). (C) Mice after resection of SiLNs. Metastases were detected in the PALN and lungs. Luciferase activity was not detected in the region of the SiLN after it had been resected. (D) Temporal changes in the luciferase activity of the PALN after resection of the SiLN. The luciferase activity of each group was normalized to the mean value of G-H6. G-D21 versus G-H6, $P < 0.05$ on day 3; G-D21 versus G-H6, $P < 0.05$ on day 28; Mann–Whitney U-test. Mean ± SD values are shown.

2.8. Statistical analysis

Data are expressed as the mean ± SD or mean ± SEM, unless otherwise indicated. Statistical comparisons were made using the Mann–Whitney U-test. Values of $P < 0.05$ were considered to be statistically significance.

3. Results

The aim was to investigate whether activation of latent metastasis in the lung was induced after resection of the SiLN inoculated with tumor cells. The potential route from the SiLN to the lung was also investigated. Fig. 1 shows the communication between the lymphatic and venous systems via SiLN. Two efferent LVs and one TV in the SiLN region can be seen in Fig. 1A. Fluorescence solution injected into the SiLN entered the TV (Fig. 1Ba), and then entered into the efferent LV (Fig. 1Bd).

Supplementary video related to this article can be found at http://dx.doi.org/10.1016/j.bbrc.2015.03.066.

In our study, the SiLN was regarded as a sentinel lymph node. We determined whether its resection influenced the growth of metastatic tumors in the lungs and PALN. Tumor cells were injected into the SiLN and bioluminescence imaging of the whole animal undertaken at various times after resection of the SiLN (Fig. 2).

Fig. 2A shows the results of bioluminescence imaging from mice in which the SiLN had been inoculated with KM-Luc/GFP cells, with subsequent resection of the SiLN either 6 h (G-H6; $n = 8$), 3 days (G-D3; $n = 4$) or 6 days (G-D6; $n = 5$) after inoculation. The control group represents mice in which the SiLN was not excised (G-C; $n = 7$). Metastasis to the PALN was induced in all groups and was evident on day 6 in the G-C, G-H6 and G-D6 groups, and on day 9 in the G-D3 group. Metastasis to the lungs was detected on day 9 in the G-H6 and G-D3 groups.

Fig. 2B shows normalized luciferase activity in the PALN for each group. The luciferase activity of the PALN increased up to day 6 and then stabilized in group G-C (no SiLN resection), whereas it increased continuously up to day 9 in mice with resected SiLNs. In group G-H6, luciferase activity of the PALN increased over time and

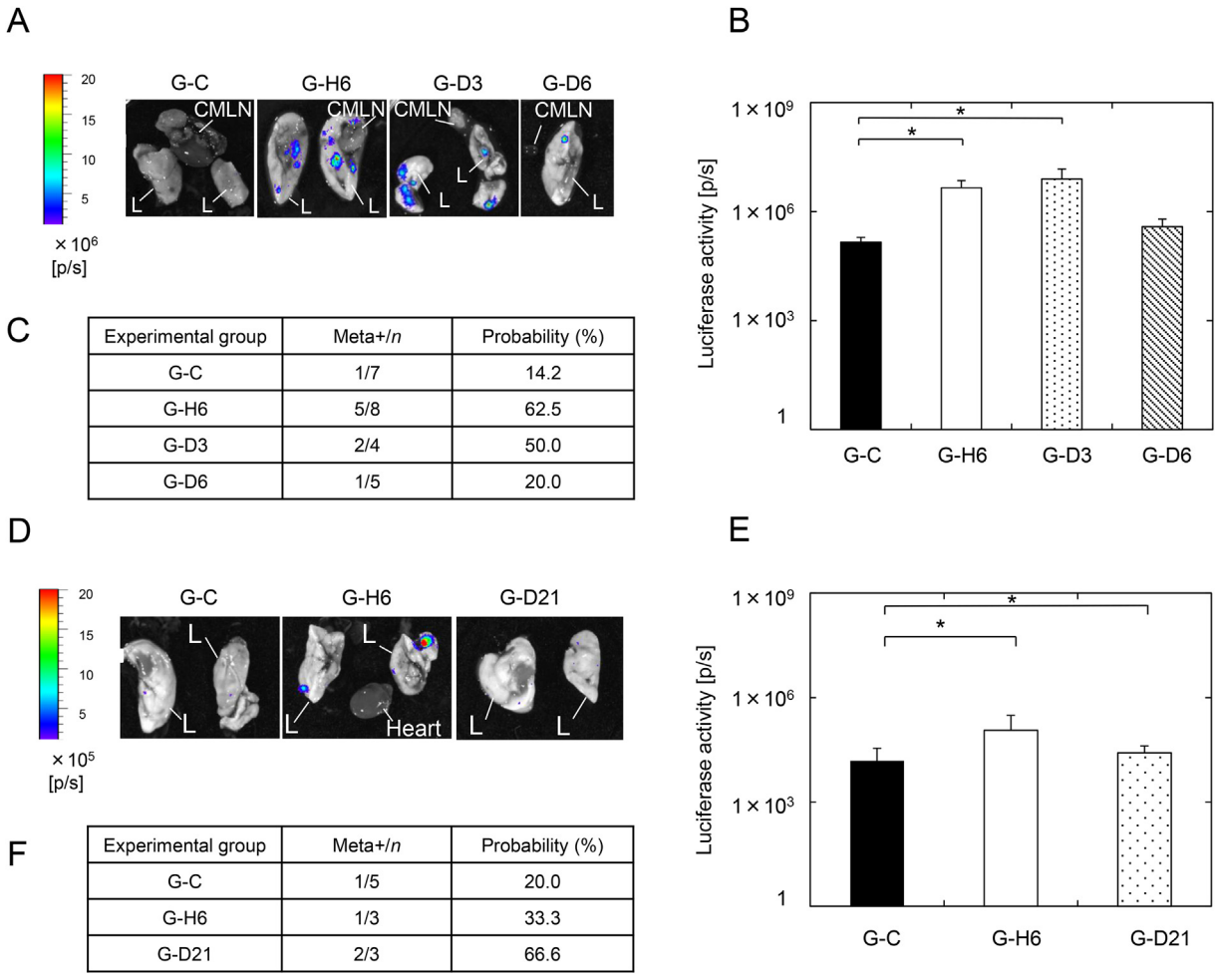

Experimental group	Meta+/*n*	Probability (%)
G-C	1/7	14.2
G-H6	5/8	62.5
G-D3	2/4	50.0
G-D6	1/5	20.0

Experimental group	Meta+/*n*	Probability (%)
G-C	1/5	20.0
G-H6	1/3	33.3
G-D21	2/3	66.6

Fig. 3. *Ex vivo* detection of metastases in the lungs using IVIS. A, B, C: KM-Luc/GFP cells. The lungs (L) and caudal mediastinal lymph node (CMLN) were removed from mice in the G-C ($n = 7$), G-H6 ($n = 8$), G-D3 ($n = 4$) and G-D6 ($n = 5$) groups on day 9. D, E, F: FM3A-Luc cells. The lungs and heart were removed from mice in the G-C ($n = 5$), G-H6 ($n = 3$) and G-D21 ($n = 3$) groups on day 28. (A) Representative *ex vivo* images of lungs and CMLN. Tumor foci were distributed discretely throughout the lungs in groups in which the SiLN had been removed (G-H6, G-D3, G-D6). More luciferase-active foci were detected in the groups having early removal of the SiLN (G-H6, G-D3). (B) *Ex vivo* luciferase activity in the PALN. Luciferase activity in the lungs was higher in the groups with early resection of the SiLN than in the control group (G-C versus G-H6, $P < 0.05$; G-C versus G-D3, $P < 0.05$). (C) Probability of detecting luciferase activity in the lungs. Probabilities were increased in the groups with early resection of the SiLN. (D) Representative *ex vivo* images of metastases in the lungs. Tumor foci were detected throughout the lungs in the G-H6 group. L: lung. (E) *Ex vivo* luciferase activity in the PALN. Luciferase activity in the lungs was higher in the groups with resection of the SiLN than in the control group (G-C versus G-H6, $P < 0.05$; G-C versus G-D21, $P < 0.05$). (F) Probability of detecting luciferase activity in the lungs. The threshold value to judge the metastasis in the lung was 1×10^5 (photons/s). Meta+: number of mice showing induction of lung metastasis; *n*: total number of mice. Mean ± SEM values are shown.

exceeded that in group G-C on day 9 ($P < 0.05$; Fig. 2B). In groups G-D3 and G-D6, luciferase activity of the PALN increased monotonically over time; on day 9, the value in group G-D6 was significantly lower than in group G-H6 ($P < 0.05$; Fig. 2B).

Fig. 2C shows the bioluminescence imaging results from mice in which the SiLN was inoculated with FM3A-Luc cells, with SiLN resection carried out either 6 h (G-H6; $n = 3$) or 21 days (G-D21; $n = 3$) after inoculation; the SiLN was not removed in the control group (G-C; $n = 5$). Metastasis to the PALN in these animals was delayed compared to mice inoculated with KM-Luc/GFP cells, and was detected on day 21 for groups G-C and G-D21, and on day 28 for group G-H6. This is likely due to FM3A-Luc cells having a slower growth rate than KM-Luc/GFP cells. The normalized luciferase activity in the PALN increased progressively over time in mice with SiLN resection (Fig. 2D), and was higher in group G-H6 compared to group G-C on day 28 ($P < 0.05$; Fig. 2D).

Metastasis to the lungs was detected in mice in which KM-Luc/GFP cells had been inoculated into the SiLN (Fig. 2A). Although not observed by IVIS, it remained possible that lung metastasis had also occurred in mice inoculated with FM3A-Luc cells. Therefore, we investigated the lung *ex vivo* by IVIS, on day 9 for KM-Luc/GFP cells and day 28 for FM3A-Luc cells (Fig. 3). In mice in which KM-Luc/GFP cells had been inoculated into the SiLN (Fig. 3A), many small metastatic foci were detected in the lungs of groups with early resection of the SiLN (G-H6, G-D3). The luciferase activity for groups G-H6 and G-D3 was significantly higher than group G-C ($P < 0.05$; Fig. 3B). The probability of metastasis to the lung was: G-H6 (62.5%) > G-D3 (50.0%) > G-D6 (20.0%) > G-C (14.2%) (Fig. 3C). In experiments using FM3A-Luc cell inoculation, small metastatic foci were detected in the lungs in group G-H6, and many metastatic foci detected throughout the entire lung in group G-D21 (Fig. 3D). Luciferase activity was significantly higher in groups G-H6 and G-D21 than in group G-C ($P < 0.05$; Fig. 3E). The probability of metastasis to the lungs was: G-D21 (66.6%) > G-H6 (33.3%) > G-C (20.0%) (Fig. 3F).

Next, the lungs were investigated histologically on day 9 for mice that had been inoculated with KM-Luc/GFP cells, and day 28 for mice inoculated with FM3A-Luc cells (Fig. 4). In experiments using KM-Luc/GFP cells (Fig. 4A and B), a metastasis with a diameter of 2 mm was detected in group G-H6, with tumor cells extravasating from the pulmonary arteries into the pulmonary parenchyma (Fig. 4Aa, b). In group G-D3, a metastasis of 200 μm diameter was observed (Fig. 4Ae). EM staining (Fig. 4Af) and CD31 (Fig. 4Ag) revealed tumor cells in the form of a tumor embolus and Matrigel in the pulmonary artery; in Fig. 4B, Matrigel is evident between the endothelium and internal elastic lamina, and endothelial and tumor cells growth in the pulmonary artery lumen. In group G-D6 (Fig. 4Ai–l), small metastatic foci were observed in the parenchyma; they presumably invaded the parenchyma from the adjacent pulmonary arteries, but the foci were not associated with the growth of CD31-positive endovascular vessels. In experiments using FM3A-Luc cells (Fig. 4C and D), tumor cells were found to have extravasated from the pulmonary arteries into the pulmonary parenchyma as shown using EM (Fig. 4Cb) and CD31 (Fig. 4Cc) staining. Tumor emboli were observed at the periphery of pulmonary arteries (Fig. 4D), and Matrigel was present in the peripheral

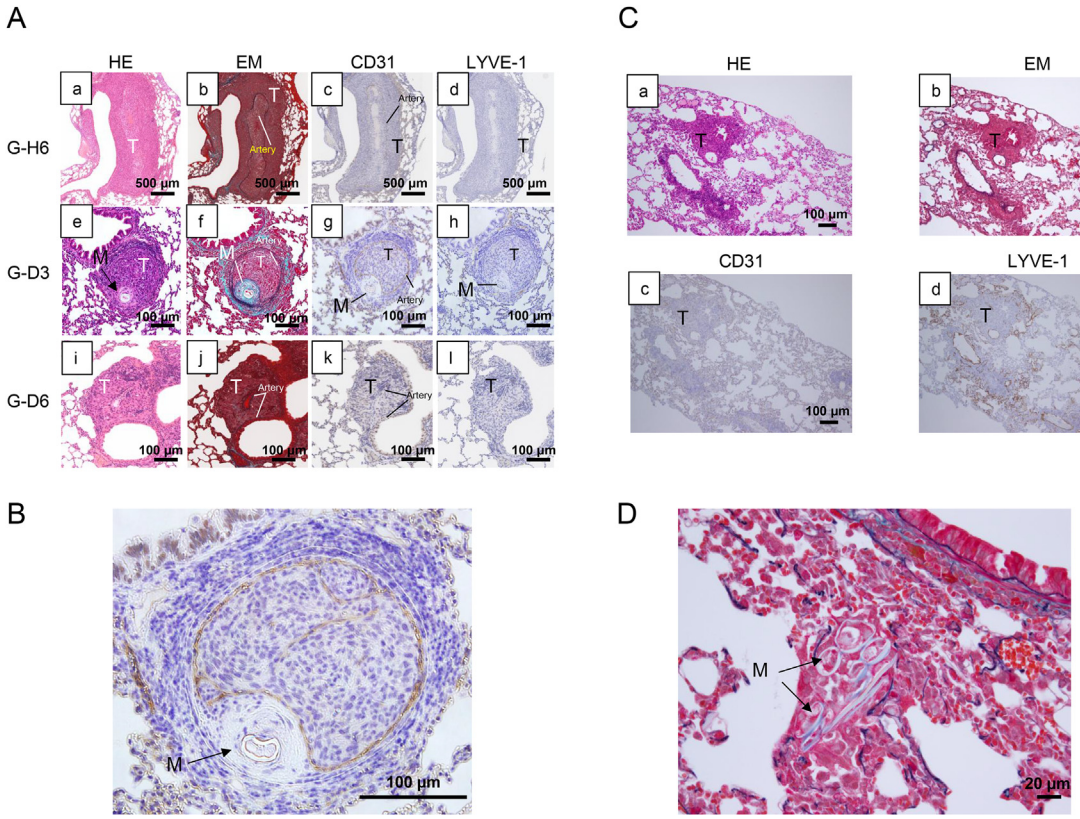

Fig. 4. Histological analysis. A, B: KM-Luc/GFP cells; C, D: FM3A-Luc cells. Samples were stained with HE, EM, anti-CD31 (CD31) or anti-LYVE-1 (LYVE-1) techniques. (A) On day 9, the lungs were dissected from mice: groups G-H6 ($n = 4$), G-D3 ($n = 4$) and G-D6 ($n = 4$). Large-sized metastatic foci were detected in group G-H6. A small amount of Matrigel (M) containing tumor cells was observed between the endothelium and internal elastic lamina of the pulmonary artery (Ae, f, g, h). (B) Magnified view of panel Ag. Tumor cells developed as a tumor embolus, which occupied the arterial lumen. Matrigel located in the subendothelial region with surrounding fibrosis, indicates an old event. (C) On day 28, the lungs were dissected from mice: group G-H6 ($n = 3$). Tumor cells (T) have extravasated from the pulmonary arteries into the pulmonary parenchyma. (D) Magnified view of an image obtained from group G-H6 (FM3A-Luc cells). Matrigel (M) was detected in the peripheral vessel.

vessel. Active CD31-positive cells related to the growth of neovascular vessels were not detected.

4. Discussion

Resection of SiLNs inoculated with tumor cells led to an accelerated growth of metastatic tumor cells in the lungs and PALN. Thus, tumor cells injected into the SiLN had clearly spread to the lungs using the venous system via the TV on the SiLN at the same time (Fig. 1). Although the flow of the fluorescence solution entering the efferent LV from SiLN in MXH10/Mo/lpr mice was visualized by our group [2], actually there were two flows; one is towards the PALN via LV, i.e. related to lymphogenous metastasis to the PALN, and the other towards the venous system by TV, i.e. it is related to hematogenous metastasis throughout the body. The lungs are the first organs to be reached by tumor cells disseminated into the venous system, with tumor cells becoming trapped in pulmonary capillaries. In the case of KM-Luc/GFP cells, tumor cells with Matrigel that had moved into the pulmonary artery were detected between the endothelium and internal elastic lamina (Fig. 4B). This finding indicates that the tumor cells existed in a latent state and had been enveloped with endothelium. They subsequently started to grow after resection of the SiLN. A similar tendency was observed for FM3A-Luc cells (Fig. 2).

Tumor latency is one stage of tumor development that lacks clinical symptoms [12]. Two mechanisms have been implicated; one involves antagonizing the expansion of a population of dividing tumor cells (tumor mass latency), and the other involves the arrest of tumor cell growth (tumor cell latency or cellular latency) [13]. We could not determine which mechanism corresponded to the latent tumor that was observed to grow in the present study.

Tumor latency occurs in primary and secondary tumors during the early stages of tumor development, in a stage of micrometastasis, and following surgical resection [14]. Recurrence of cancer frequently occurs after treatment or long periods of remission. For instance, 20–45% of patients with breast or prostate cancer will relapse a few years or even decades later [13], because latent tumor cells that remain after removal or treatment of the primary tumor are resistant to chemotherapy.

In our study, tumor cells in the metastasis sites (i.e., PALN or lung) were activated in mice in which the SiLN had been resected 6 h, 3 days or 6 days after inoculation of KM-Luc/GFP cells, and 6 h or 21 days after inoculation of FM3A-Luc cells. This activation of tumor cells is consistent with previous results suggesting that tumor latency could occur at an early stage of tumor development [15].

The concentration of serum VEGF increases and serum endostatin decreases, after pulmonary/breast surgery [16]. These changes may well accelerate the growth of a latent tumor [5]. In our study, the proliferation of CD31-positive endothelial cells, an indicator of active neovascularization, was not detected in pulmonary metastatic foci. Thus, it is unlikely that the accelerated growth of metastatic foci was triggered by the proliferation of tumor neovascular vessels. It may be that tumor neovascular vessels are not required for tumor growth because of the abundant blood flow in the pulmonary parenchyma. Dillekas and colleagues [17] have hypothesized that multiple similar-sized metastases, at the time of first recurrence, occur due to synchronized growth kinetics. It will be interesting to extend the present study by investigating the size distribution of the metastatic foci in the lungs.

In conclusion, the experimental mouse model described here allowed observations on the activation and development of microscopic metastasis foci, which occurred after LN resection, in a reproducible fashion and in a real-time basis. This model may prove to be very useful for the elucidation of the mechanisms of tumor latency and for the development of methods to either extend the latent state, inhibit tumorigenesis at an early stage, or prevent the formation of metastases.

Conflict of interest

The authors declare that there are no conflicts of interest.

Acknowledgments

We are grateful to M. Nose for providing technical advice on pathological analysis. This study was supported in part by JSPS KAKENHI Grant Numbers 26293425 (SM), 26670856 (SM), 25293382 (MS), 24659834 (MS), 26242051 (TK) and 24650286 (TK). LS was supported by the JSPS Dissertation PhD Program (TK).

Transparency document

Transparency document related to this article can be found online at http://dx.doi.org/10.1016/j.bbrc.2015.03.066.

References

[1] K. Kawada, M.M. Taketo, Significance and mechanism of lymph node metastasis in cancer progression, Cancer Res. 71 (2011) 1214–1218.
[2] T. Kodama, Y. Hatakeyama, S. Kato, S. Mori, Visualization of fluid drainage pathways in lymphatic vessels and lymph nodes using a mouse model to test a lymphatic drug delivery system, J. Biomed. Opt. 6 (2015) 124–134.
[3] R. Demicheli, M.W. Retsky, W.J. Hrushesky, M. Baum, Tumor dormancy and surgery-driven interruption of dormancy in breast cancer: learning from failures, nature clinical practice, Oncology 4 (2007) 699–710.
[4] E. Tagliabue, R. Agresti, M.L. Carcangiu, C. Ghirelli, D. Morelli, M. Campiglio, M. Martel, R. Giovanazzi, M. Greco, A. Balsari, S. Menard, Role of HER2 in wound-induced breast carcinoma proliferation, Lancet 362 (2003) 527–533.
[5] Y. Maniwa, M. Okada, N. Ishii, K. Kiyooka, Vascular endothelial growth factor increased by pulmonary surgery accelerates the growth of micrometastases in metastatic lung cancer, Chest 114 (1998) 1668–1675.
[6] D. Sano, M.K. Gule, D.I. Rosenthal, D. Bell, J. Yates, A.K. El-Naggar, J.N. Myers, Early postoperative epidermal growth factor receptor inhibition: safety and effectiveness in inhibiting microscopic residual of oral squamous cell carcinoma in vivo, Head. Neck 35 (2013) 321–328.
[7] B. Fisher, N. Gunduz, J. Coyle, C. Rudock, E. Saffer, Presence of a growth-stimulating factor in serum following primary tumor removal in mice, Cancer Res. 49 (1989) 1996–2001.
[8] L. Shao, S. Mori, Y. Yagishita, T. Okuno, Y. Hatakeyama, T. Sato, T. Kodama, Lymphatic mapping of mice with systemic lymphoproliferative disorder: usefulness as an inter-lymph node metastasis model of cancer, J. Immunol. Methods 389 (2013) 69–78.
[9] T. Sato, S. Mori, Y. Arai, T. Kodama, The combination of intralymphatic chemotherapy with ultrasound and nano-/microbubbles is efficient in the treatment of experimental tumors in mouse lymph nodes, Ultrasound Med. Biol. 40 (2014) 1237–1249.
[10] W. Van den Broeck, A. Derore, P. Simoens, Anatomy and nomenclature of murine lymph nodes: descriptive study and nomenclatory standardization in BALB/cAnNCrl mice, J. Immunol. Methods 312 (2006) 12–19.
[11] L. Li, S. Mori, M. Kodama, M. Sakamoto, S. Takahashi, T. Kodama, Enhanced sonographic imaging to diagnose lymph node metastasis: importance of blood vessel volume and density, Cancer Res. 73 (2013) 2082–2092.
[12] J. Li, E. Jiang, X. Wang, A.J. Shangguan, L. Zhang, Z. Yu, Dormant cells: the original cause of tumor recurrence and metastasis, Cell. Biochem. Biophys. (2015 Jan 3) [Epub ahead of print].
[13] J.A. Aguirre-Ghiso, Models, mechanisms and clinical evidence for cancer dormancy, Nat. Rev. Cancer 7 (2007) 834–846.
[14] S.S. Qadri, J.H. Wang, J.C. Coffey, M. Alam, A. O'Donnell, T. Aherne, H.P. Redmond, Can surgery for cancer accelerate the progression of secondary tumors within residual minimal disease at both local and systemic levels? Ann. Thorac. Surg. 80 (2005) 1046–1050 discussion 1050–1041.
[15] P.T. Logan, B.F. Fernandes, S. Di Cesare, J.C. Marshall, S.C. Maloney, M.N. Burnier Jr., Single-cell tumor dormancy model of uveal melanoma, Clin. Exp. Metastasis 25 (2008) 509–516.
[16] F.P. Wu, K. Hoekman, S. Meijer, M.A. Cuesta, VEGF and endostatin levels in wound fluid and plasma after breast surgery, Angiogenesis 6 (2003) 255–257.
[17] H. Dillekas, M. Transeth, M. Pilskog, J. Assmus, O. Straume, Differences in metastatic patterns in relation to time between primary surgery and first relapse from breast cancer suggest synchronized growth of dormant micrometastases, Breast Cancer Res. Treat. 146 (2014) 627–636.